CROATICA CHEMICA ACTA CCACAA **62** (4) 835—853 (1989)

YU ISSN 0011-1643
CCA-1911 UDC 541
Conference Paper

A Study of Solid-Liquid Interface by Computer Simulation

Gojko Balabanić[1], Branko Borštnik[2], Radovan Milčić[3], Antun Rubčić[4], and Franjo Sokolić[5]

[1]*Civil Engineering Institute, Rijeka*
[2]*»Boris Kidrič« Institute of Chemistry, Ljubljana*
[3]*Civil Engineering Institute, Zagreb*
[4]*Faculty of Science, University of Zagreb, POB 162, Zagreb*
[5]*»Ruđer Bošković« Institute, POB 1016, Zagreb, Yugoslavia*

Received February 6, 1989

The Monte Carlo simulation technique is applied to the study of two models of solid-liquid interface: Lennard-Jones fluid near a hard and soft plane wall. The following characteristic physical quantities for elucidation of the behaviour of the fluid in the interface region were calculated: density profiles, pair correlation functions, potential energy profiles, profiles of the pressure tensor components, surface tension and excess values of number density, potential energy and entropy density. All these quantities were calculated at different thermodynamic points in order to establish their dependence on the temperature and density. An unexpected result is that a hard wall in its vicinity induces a decrease of the order in the Lennard-Jones fluid in contrast to that of a soft wall.

1. INTRODUCTION

In the past decade there was a revial of interest for interfacial phenomena. The field of physical chemistry of surfaces encompassing the phenomenological description of interfacial phenomena (mechanical and thermodynamical) has undergone qualitative change due to the advent of computer simulation. This has enabled a much more thorough study of these phenomena on microscopic level. Finally, reliable microscopic data have appeared, enabling the validity of different approaches and approximations of the statistical mechanics of surfaces to be estimated.

Solid-fluid interface is of particular interest for different applications such as electrode processes, lubrication, crystal nucleation and growth, melting, chromatography, oil recovery, membrane separation technologies, colloid solutions, etc. The physical aspects of these applications cover the structural and dynamic properties of liquids in contact with substrate and processes which involve the phase changes, such as melting and crystal nucleation and growth.

An analysis of the solid-liquid interface on the microscopic level can be performed by computer simulation methods or by solving the appropriate

integral equations of statistical mechanics. For a given model the simulation results may be considered as experimental.

Because of the computational and theoretical difficulties encountered when treating the interfacial phenomena, only simple models have been thoroughly investigated so far. The liquid phase was usually taken to be pure, consisting of monoatomic particles such as hard spheres (HS) or Lennard-Jones (L-J) particles. Concerning the solid phase, both geometry and microscopic structure should be specified. This is determined by the problem under investigation. The liquid-solid interaction potential is the crucial parameter determining the interfacial properties. This may be considered to be the sum of direct interactions of a particle in a liquid with those in a solid or an interaction through some mean field potential. In the latter case, the solid acts like a wall and the interaction depends only on the distance from it.

Although considerable attention has been paid to such systems, a complete unambiguous physical picture has not yet been reached. This has stimulated our interest in these systems, having in mind that no real progress can be made without a complete understanding of simple models.

One unresolved problem was that concerning the influence of the wall on the structure of the fluid. This is described by two principal physical quantities, the density profile and the pair correllation function.

Additional quantities determining the state of the system are thermodynamic properties. Besides the values characterizing the global state of the system, we can also look at their local variation. This takes us into the realm of local thermodynamics. We pay particular attention to the analysis of such quantities in order to understand what is going on in fluid layers at the interface.

2. MODELS AND PREVIOUS RESULTS

Because of some of its specific features we paid particular attention to the analysis of the L-J fluid-hard wall (L-J/HW) system. L-J fluid consists of particles interacting through the potential

$$u_2(r) = 4\varepsilon\left((\sigma/r)^{12} - (\sigma/r)^6\right) \tag{1}$$

The fluid particle interacts with a hard wall through the potential

$$u_1(z) = \begin{cases} 0 & z > 0 \\ \infty & z \leqslant 0 \end{cases} \tag{2}$$

The behaviour of the bulk L-J fluid is described by its phase diagram, given in Figure 1. Two different liquid-vapour coexistence lines, that of a L-J fluid where long range corrections are taken into account[1] and that of a L-J fluid where a cut-off radius of 2.5 σ is used[2], which is more appropriate for our model.

Irrespective of the values of ε and σ parameters in each particular case, all thermodynamic points can be represented in the same diagram, where reduced quantities are given on the coordinate axes. The reduced quantities have no dimension and in the particular case of length, temperature, density and pressure are given by

$$r^* = r/\sigma,\ T^* = kT/\varepsilon,\ \varrho^* = \varrho\sigma^3,\ p^* = p\sigma^3/\varepsilon \tag{3}$$

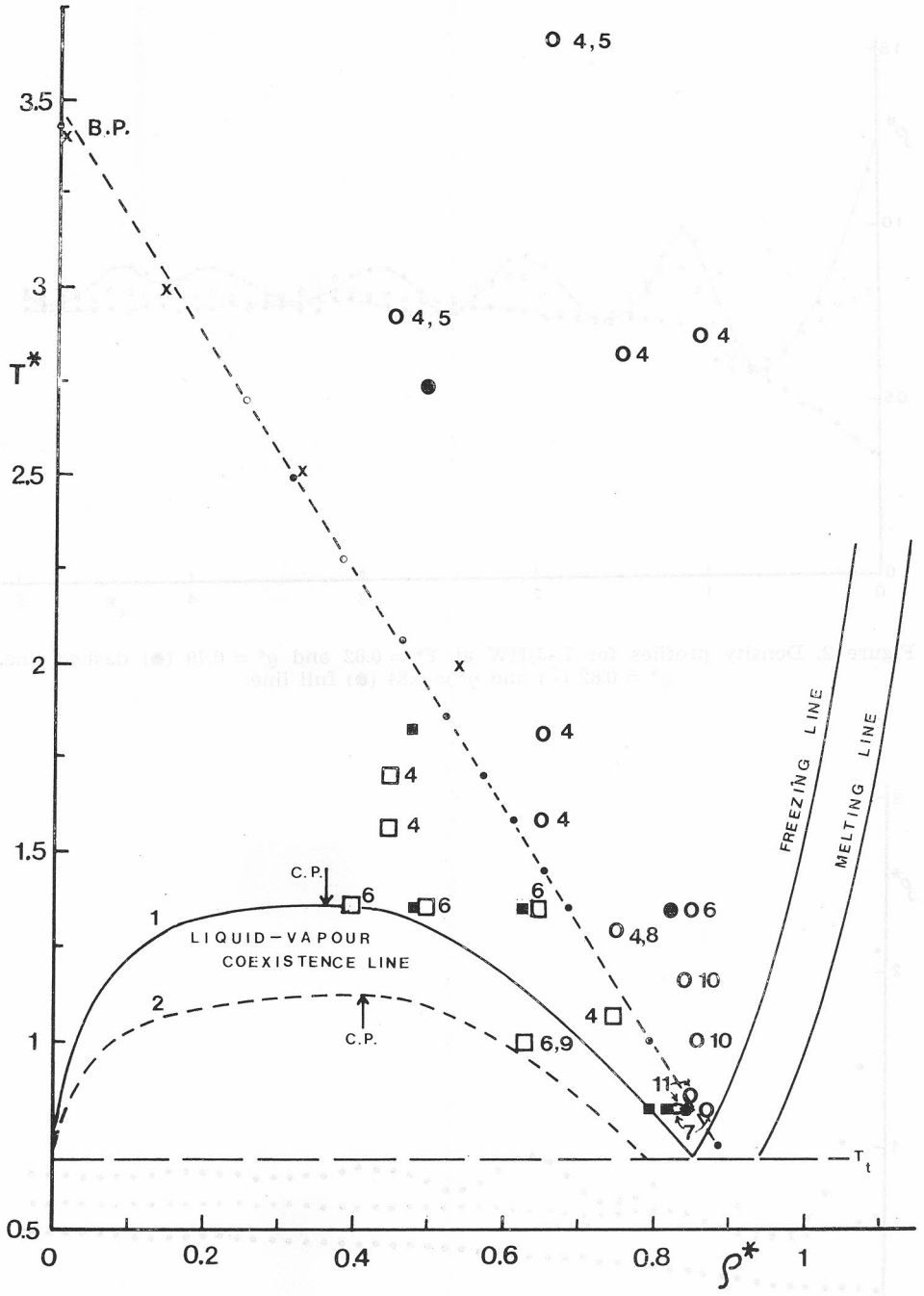

Figure 1. Phase diagram for L-J fluid. Squares (continuous density profile) and circles (oscillatory density profile) represent points at which calculations were performed by us (full) and other authors (open). Attached numbers represent cardinal numbers of the corresponding references. Crosses and dots represent points where condition $\varrho_b = \varrho(0)$ is fulfilled, as described in the text, and the straight dashed line divides phase points where continuous and oscillatory density profiles are found.

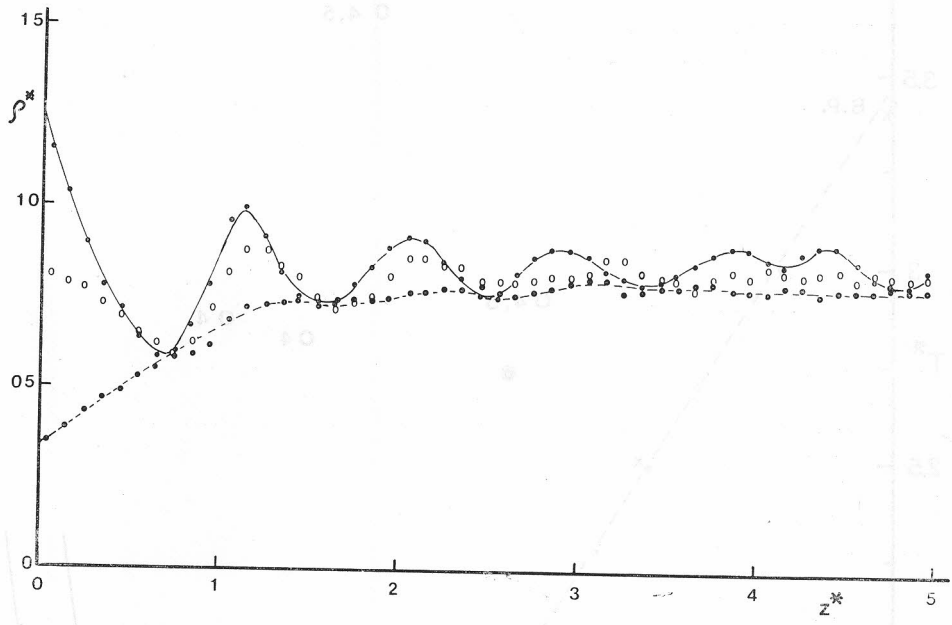

Figure 2. Density profiles for L-J/HW at $T^* = 0.82$ and $\varrho^* = 0.79$ (●) dashed line, $\varrho^* = 0.82$ (○) and $\varrho^* = 0.84$ (●) full line.

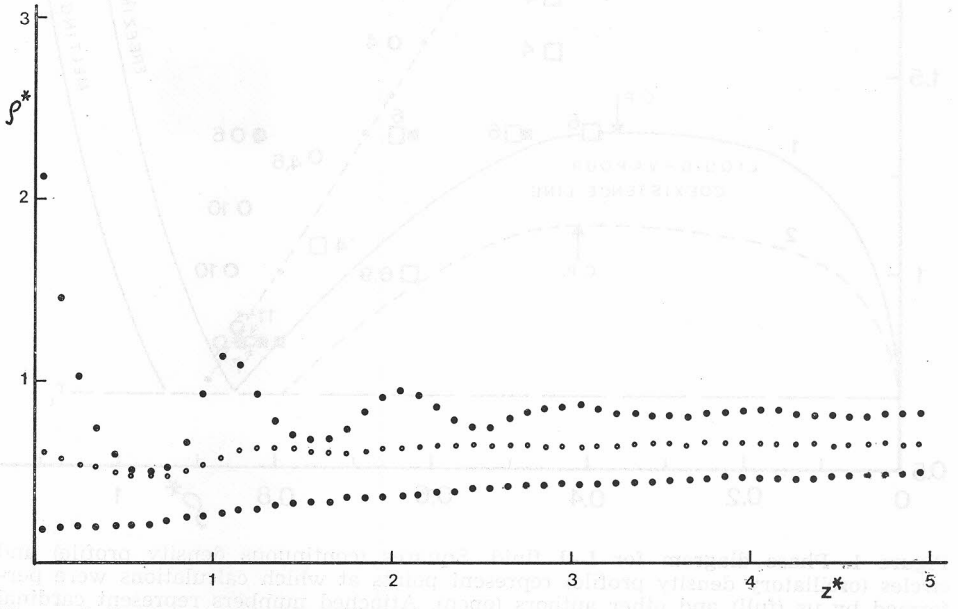

Figure 3. Density profiles for L-J/HW at $T^* = 1.35$ and $\varrho^* = 0.5$, 0.63 and 0.82 going from the bottom to the top.

Inhomogeneous fluid at different thermodynamic points can also be represented in the same phase diagram. The structure of such a fluid is characterized by a variation of the local number density $\rho(z)$ with the distance from the wall, which is supposed to be in the z direction. This density profile has two different characteristic forms, as it will be shown in the next section (see Figures 2 and 3). In one case $\rho(z)$ raises continuously to its bulk value, while in the other case it oscillates in the vicinity of the wall. The oscillations die out completely at a distance of several σ from the wall, reaching the bulk density value. Which behaviour is attained depends on the thermodynamic point in which the bulk fluid is found. The continuous density profile corresponds to the states where the temperature and/or density is low. In these conditions the attractive part of the fluid particles interaction is dominant, and a low density fluid is intertwined between the solid and liquid phase. The oscillatory density profile corresponds to the high temperature and/or high density conditions. Now the repulsive part of the potential becomes dominant causing a layering of the fluid next to the wall.

Although several authors performed calculations of $\rho(z)$ for this system, their thermodynamic points were chosen randomly and no attempt was made to try to find the position of the transition region between these two characteristic regimes.

With the aim of elucidating the position of this transition region we reproduced the already existing results for $\rho(z)$ at different points of the phase diagram in the following way: for continuous $\rho(z)$ by sign □ and for oscillatory by ○. The transition region is situated in the vicinity of the line connecting the triple point with the point at the Boyle temperature and zero density. This line may be approximated by the equality of the bulk ρ_b and the contact density $\rho(0)$. The contact density represents the extrapolation of the density profile to the wall. At low density this equality may be determined from the virial equation of state up to the fifth virial coefficient, which are all known for L-J fluid[3]

$$\frac{p}{kT} = \varrho + \sum_{i=2}^{5} B_i(T)\,\varrho^i \tag{4}$$

The equality of ρ_b and $\rho(0)$ corresponds to the states where the sum in eq. (4) vanishes. The corresponding algebraic equations are solved numerically and the results are shown by crosses (×) in Figure 1. Crosses lie on a straight line for low densities but, as expected, deviate considerably for higher ones.

Another way of obtaining this line of separation of two density profiles is by the Monte Carlo (MC) simulation. If we draw the isotherms in the $(p/\rho\,kT,\ \rho)$ diagram and look for the intersections with the straight line $p/\rho\,kT = 1$, then these points correspond to the condition $\rho_b = \rho(0)$, and are represented by dots (●) in Figure 1.

The results given in Figure 1 have been obtained by different methods. The integral BGYB hierarchy of equations is solved in refs. 4 and 5. The singlet and self-consistent Percus-Yevick theory are applied in ref. 6. Density functional theory is used in refs. 7 and 8. MC simulation results are given in refs. 9, 10 and in 11 for a slightly modified L-J potential.

The width of the transition region is very narrow in the vicinity of the triple point, as shown in refs. 7 and 11, and broadens by approaching the Boyle temperature.

Some calculations were also performed for the L-J fluid in contact with a soft wall (L-J/StW) whose potential is defined by[12]

$$u_1(z) = A\left[\frac{2}{5}(\sigma/z)^{10} - (\sigma/z)^4 - \frac{\sigma^4}{3\Delta\,(z+0.61\Delta)^3}\right] \tag{5}$$

where Δ is the interplane distance in a crystal. In our calculation $\Delta = \sigma/\sqrt{2}$ and $A = 2\pi\varepsilon$. For this system previous MC calculations were performed in refs. 8, 10 and 13. The density functional theory is also used.[8,13]

In this paper we use the MC technique to simulate a system of 384 L-J particles confined by two parallel plane walls located at $z = 0$ and $z = 3L$. The periodic boundary conditions are applied in x and y direction with periodicity length equal to L. The quantity L was determined from $L = {}^3\sqrt{N/3\rho}$, where N is the total number of particles, and ρ is the average number density. In the presentation of results for L-J/HW system the origin of the z coordinate is shifted for $\sigma/2$ to the right to conform with the presentation in other references.

Because of the nonuniform distribution of density caused by the presence of the wall and the finite size of the system, the average density does not represent the appropriate quantity to fix the thermodynamic point. Instead, the bulk density ρ_b is introduced, representing the density of the fluid in the region without the wall effects. These two densities coincide in the thermodynamic limit. Results obtained in systems of different sizes should be compared at equal bulk density. This quantity appears as an asymptotic value of density far from the wall in an equilibrated MC configuration.

Interaction of two particles is considered only if their mutual distance is smaller than the cut-off radius $r_c = L/2$. The nearest image convention is used.

The most important calculated properties are the density profile $\rho(z)$ and the pair correlation function (PCF), $g(z_i, z_j, r_{ij})$. The density profile is determined by dividing the system into panels parallel to the xy plane of the width $\Delta z = 0.1\,\sigma$, and then counting the number of particles N_i in the i-th panel and averaging it over a large number of configuratios, *i. e.*

$$(z_i) = \frac{\langle N_i \rangle}{V_i} \tag{6}$$

V_i being the volume of the panel and z_i the z-coordinate of the center of the i-th panel.

The PCF given by the relation

$$g(z_i, z_j, r_{ij}) = \frac{2\langle N_{ij} \rangle}{\varrho(z_i)\,\varrho(z_j)\,L^2\,\Delta z\,\Delta V} \tag{7}$$

is calculated in the following way: a spherical shell of the mean radius r and thickness Δr is circumscribed around the reference particle in the i-th

panel. We look for the number of particles in volume ΔV common to this shell and the j-th panel. Averaging is performed over different configurations. In our calculation $\Delta r = 0.1\,\sigma$.

The starting configuration for a MC run was taken to be the fcc crystal lattice or a configuration generated by a previous calculation in another thermodynamic point. Equilibration is attained after 4—5 million configurations in the case of inhomogeneous liquid or 500 thousand in the case of the bulk liquid. Averaging is performed over additional several tenths of millions of configurations by picking up one after each 2000 configurations to calculate the physical quantity we are looking for. The maximum particle displacement is taken to be 35 pm and 50 pm, at high and low densities, respectively, so that the acceptance ratio of 40—70% is attained.

We have analyzed the dependence of the obtained results on the number of particles in the system. We have used systems with 192[14] and 384 particles. Density profile appeared to be non-sensitive to this change, while PCF changed slightly, showing in the latter case complete agreement of our bulk PCF's with those obtained by other authors.[15]

3. RESULTS AND DISCUSSION

Our aim is to study the behaviour of a L-J fluid in contact with a single plane wall. Although we have been using a MC cell with two walls, in our calculation, the distance between is chosen to be large enough to eliminate the mutual interference of their effects. This was checked by calculating the PCF in the central region of the cell, which corresponded exactly to the bulk PCF under the same thermodynamic conditions.

a) Density Profile

In order to determine the density and temperature dependence of the properties of our system we have chosen the thermodynamic points on the isotherms at $T^* = 0.82$, 1.35 and 2.74, and the isochores at approximately $\rho^* = 0.5$ and 0.82. Some results are given in a previous work[16].

In Figure 2 the density profiles at three different densities, $\rho^* = 0.79$, 0.82 and 0.84 and temperature $T^* = 0.82$, are shown. As discussed in Section 2, there are two characteristic forms of density profile (continuous and oscillatory), with a very narrow transition region.

Density profiles at higher temperature $T^* = 1.35$ and three different densities, $\rho^* = 0.5$, 0.63 and 0.82, are given in Figure 3. We can notice that the transition region in this case is much broader. The width of this transition region is proportional to the derivative of the isotherm at the point where it intersects the line $p/\rho kT = 1$. Above the Boyle temperature ($T_B^* = 3.4$), there is no such intersection and consequently only one characteristic shape, oscillatory or quasioscillatory (at low densities), of the density profile exists.

In Figure 4 density profiles for three different temperatures, $T^* = 1.35$, 1.71 and 2.74, and at approximately the same density $\rho^* \doteq 0.5$, are given. When comparing the density profiles for one density and growing temperatures, one can notice the growth of contact density.

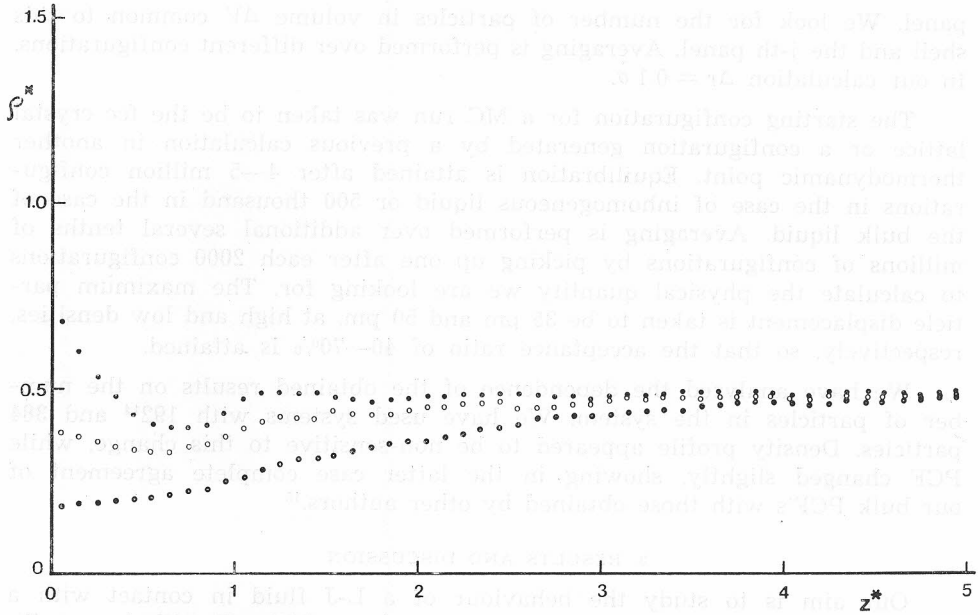

Figure 4. Density profiles for L-J/HW at $\varrho^* = 0.5$ and $T^* = 1.35$ (●), 1.71 (○) and 2.74 (●) going from the bottom to the top.

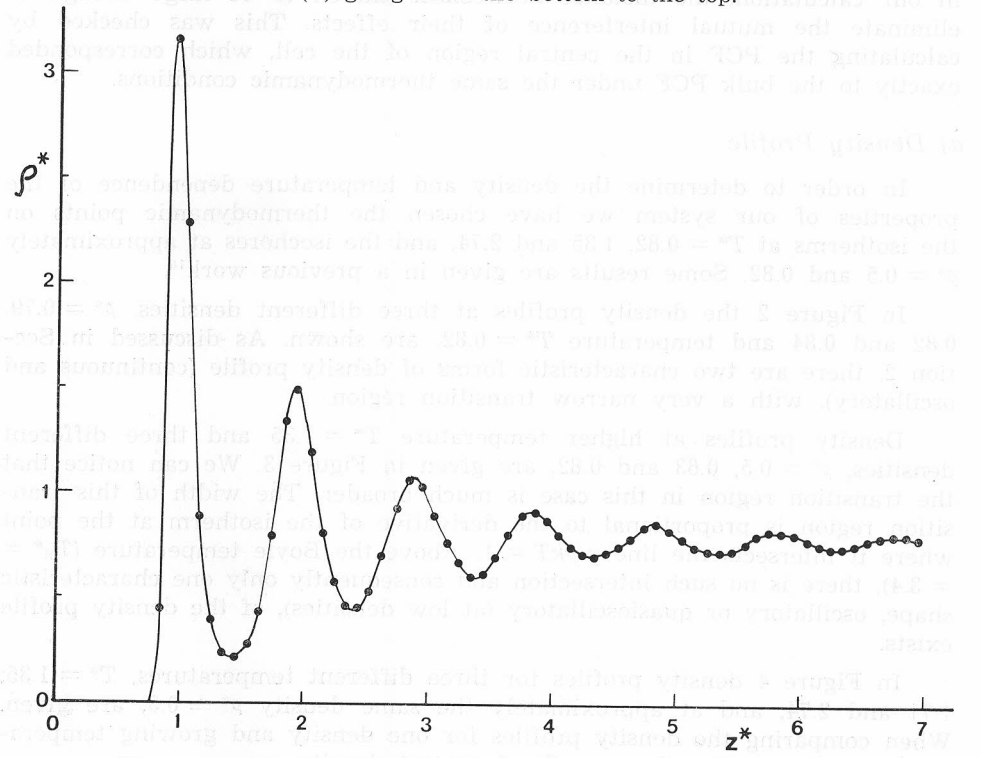

Figure 5. Density profile for L-J/StW at $T^* = 1.17$ and $\varrho^* = 0.78$.

In Figures 2 and 3 it can be observed that the distance between the first maximum and the first minimum is larger than the corresponding distance in subsequent layers. With increasing temperature this distance decreases tending to the limiting value of $\sigma/2$.

Density profile for the case of L-J/StW system at $T^* = 1.17$ and $\rho^* = 0.78$ is given in Figure 5. In this case density profile has a more pronounced oscillatory character (particularly the first maximum is higher, due to the attractive part of the potential) with respect to that of the L-J/HW system in a close thermodynamic point. In contrast to the hard wall, the soft wall gives all layers of equal width.

b) Pair Correlation Function

The structural details of the L-J fluid at various distances from the wall were elucidated by the calculation of PCF's. For the inhomogeneous fluid the PCF is not isotropic. In this study particular attention was paid to the analysis of PCF's in directions parallel to the wall. PCF's for three different panels, of the width $0.1\,\sigma$, parallel to the wall at the thermodynamic point $T^* = 1.35$, $\rho^* = 0.82$ are represented in Figure 6. Figure 7 gives the correlation of the first with subsequent panels. Figure 8 gives the correlation in all directions. The left side represents the correlation in the direction parallel to the wall within the first panel, as in Figure 6. The middle part represents the correlation between one particle in contact with the wall, while the other is at a distance corresponding to the maximum of the PCF's for different angles between their relative radius vector and the plane of the wall (see Figure 7). The right part represents the PCF orthogonal to the wall.

In Figure 9 PCF's for different panels parallel to the wall for the L-J/StW system at thermodynamic point $T^* = 1.17$, $\rho^* = 0.78$ are shown.

The common feature of the PCF's for the contact layer for both L-J/HW and L-J/StW systems is a shift of the second maximum and the first and second minimum as it may be seen from Figures 6 and 9. By increasing the distance of the panel from the wall there is a continuous transition of the form of the PCF to its bulk form (see Figures 6 and 9). The same effect is also seen in Figure 7 for the second peak while the first peak shows a different behaviour concerning the height of its maximum, which is also seen from the central part of Figure 8. The maximum in the central part corresponds to the most probable orientation of the line connecting one particle in the contact layer and its first neighbours with respect to the wall.

The shift of maxima and minima was already noticed for HS/HW system[17,18]. In ref. 17 it was pointed out that this may be a consequence of the two-dimensional (2D) character of the contact layer. This is confirmed by the finding[19] that the self-diffusion coefficient for the HS/HW system is smaller in the direction orthogonal to the wall with respect to that parallel to the wall. Calculation[20] of the mean potential for a HS as a function of the distance from the HW points to the existence of a relatively high potential barrier between the first and the second layer with respect to those between other layers.

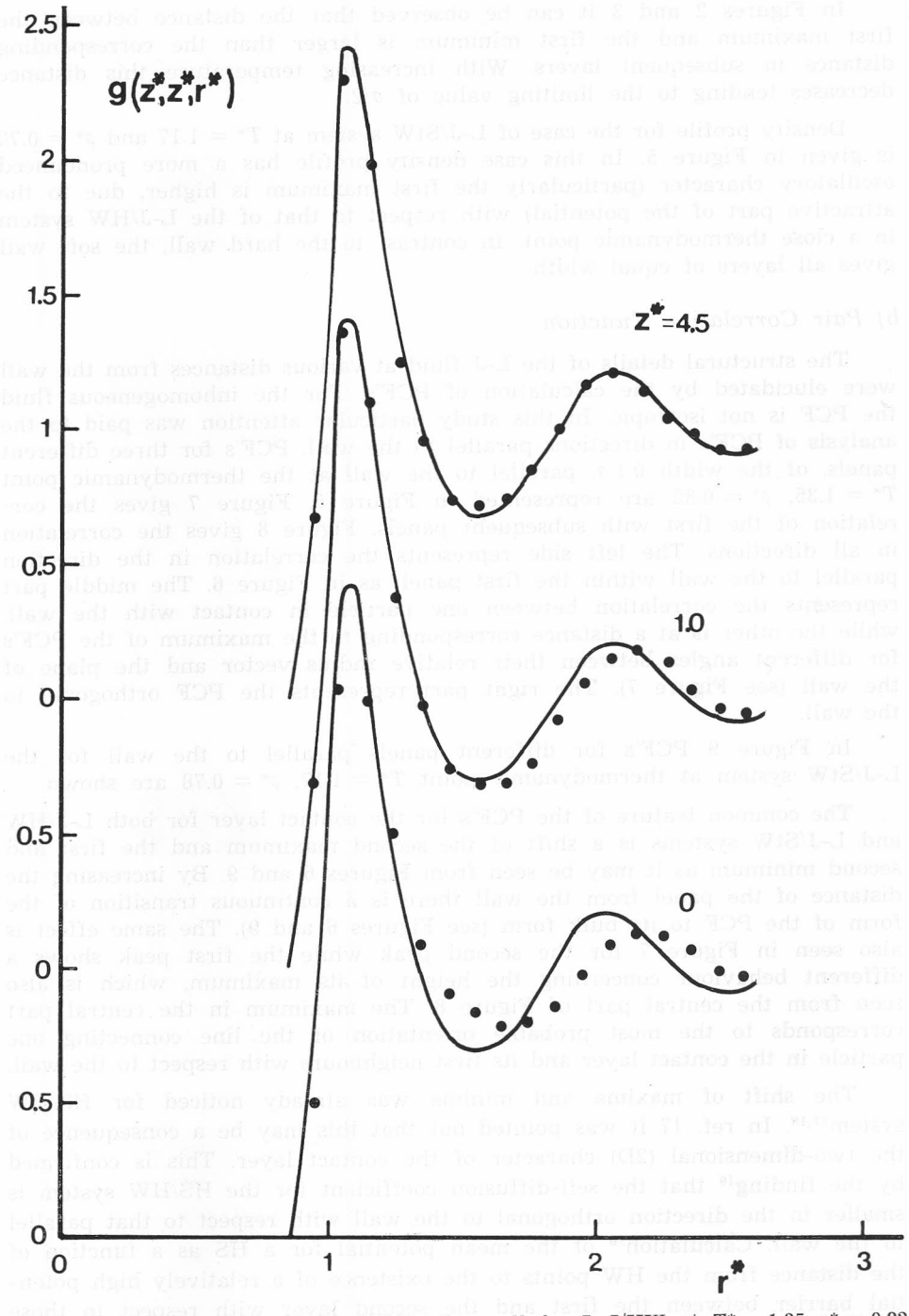

Figure 6. PCF's for panels parallel to the wall for L-J/HW at $T^* = 1.35$ $\varrho^* = 0.82$ at distances $z^* = 0$, 1.0 and 4.5 from the wall (dots) and bulk PCF (full line).

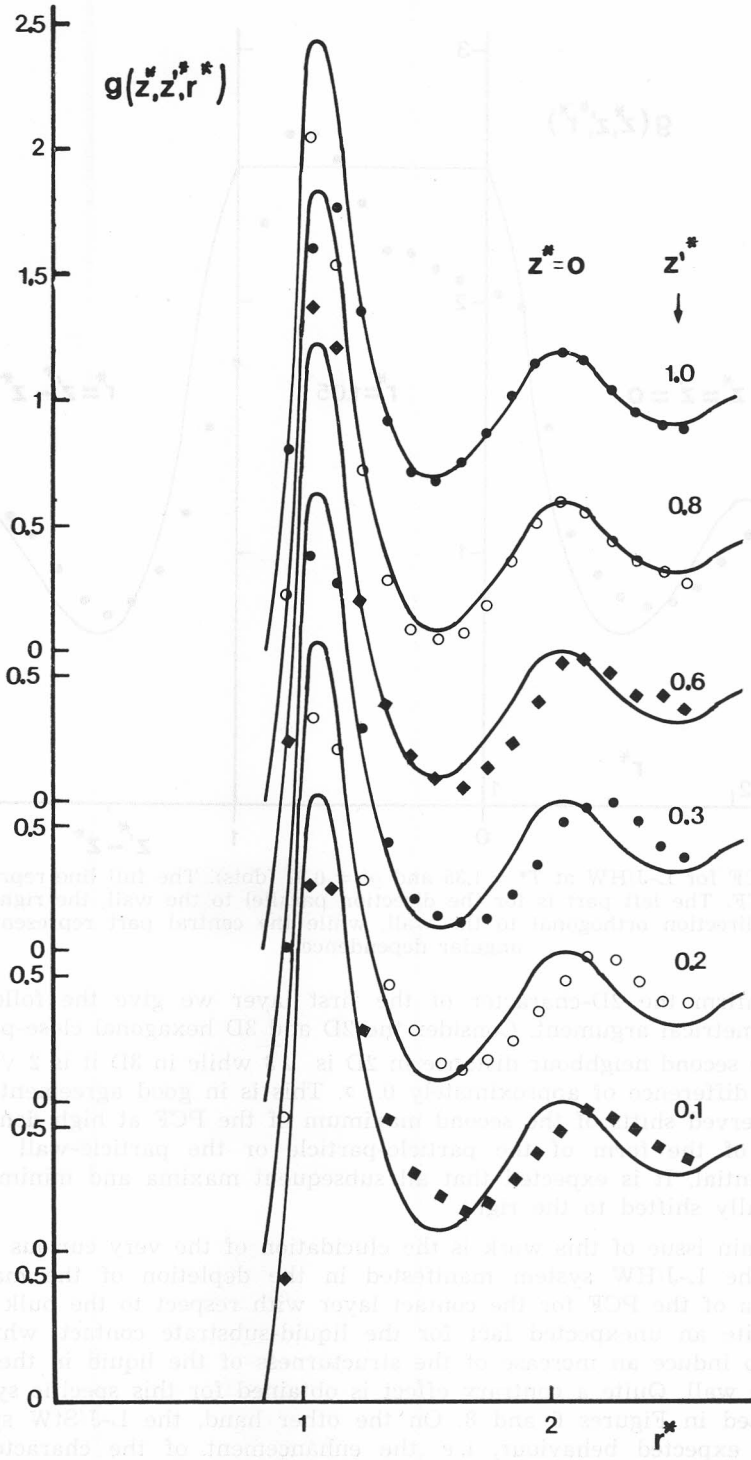

Figure 7. PCF's for one particle in the contact layer ($Z^* = 0$) and the other at $z'^* =$ $= 0.1$, 0.2, 0.3, 0.6, 0.8, and 1.0 for L-J/HW at $T^* = 1.35$ and $\varrho^* = 0.82$ (symbols) and bulk PCF (full line).

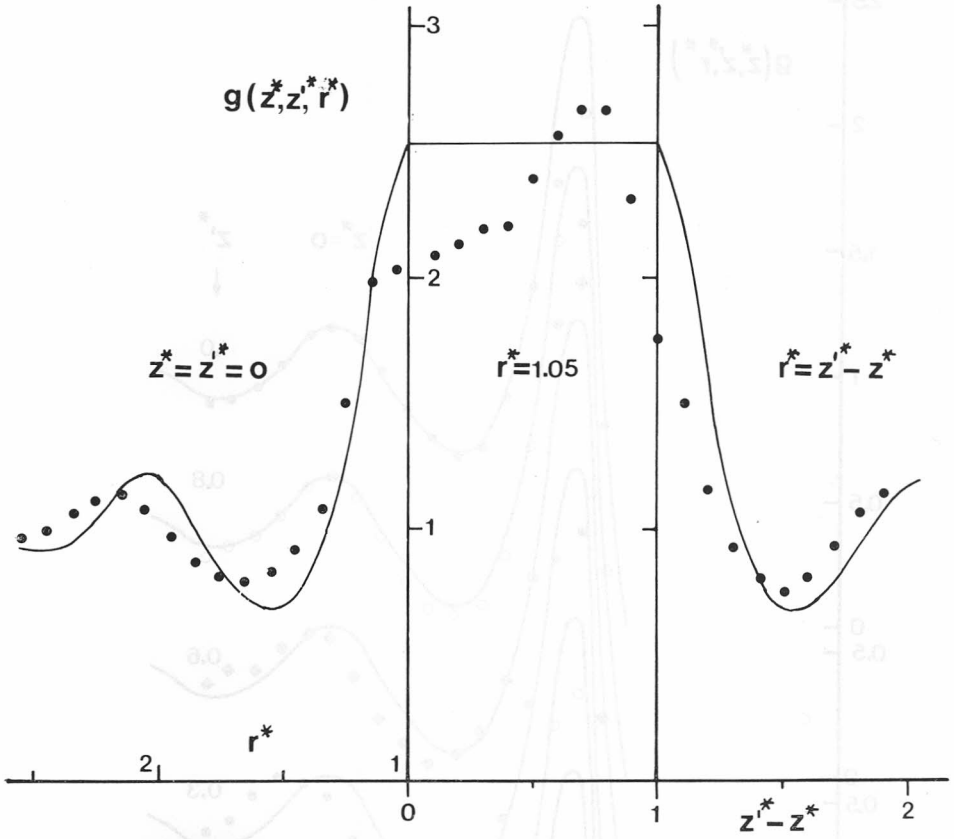

Figure 8. PCF for L-J/HW at $T^* = 1.35$ and $\varrho^* = 0.82$ (dots). The full line represents the bulk PCF. The left part is for the direction parallel to the wall, the right part is for the direction orthogonal to the wall, while the central part represents the angular dependence.

To confirm the 2D-character of the first layer we give the following simple geometrical argument. Consider the 2D and 3D hexagonal close-packed lattice. The second neighbour distance in 2D is $\sqrt{3}$ while in 3D it is $2\sqrt{2/3}\,\sigma$, giving the difference of approximately $0.1\,\sigma$. This is in good agreement with all the observed shifts of the second maximum of the PCF at high densities, regardless of the form of the particle-particle or the particle-wall interaction potential. It is expected that all subsequent maxima and minima are proportionally shifted to the right.

The main issue of this work is the elucidation of the very curious behaviour of the L-J/HW system manifested in the depletion of the maxima and minima of the PCF for the contact layer with respect to the bulk PCF. This is quite an unexpected fact for the liquid-substrate contact, which is expected to induce an increase of the structurness of the liquid in the vicinity of the wall. Quite a contrary effect is obtained for this specific system, as illustrated in Figures 6 and 8. On the other hand, the L-J/StW system shows the expected behaviour, *i. e.* the enhancement of the characteristic

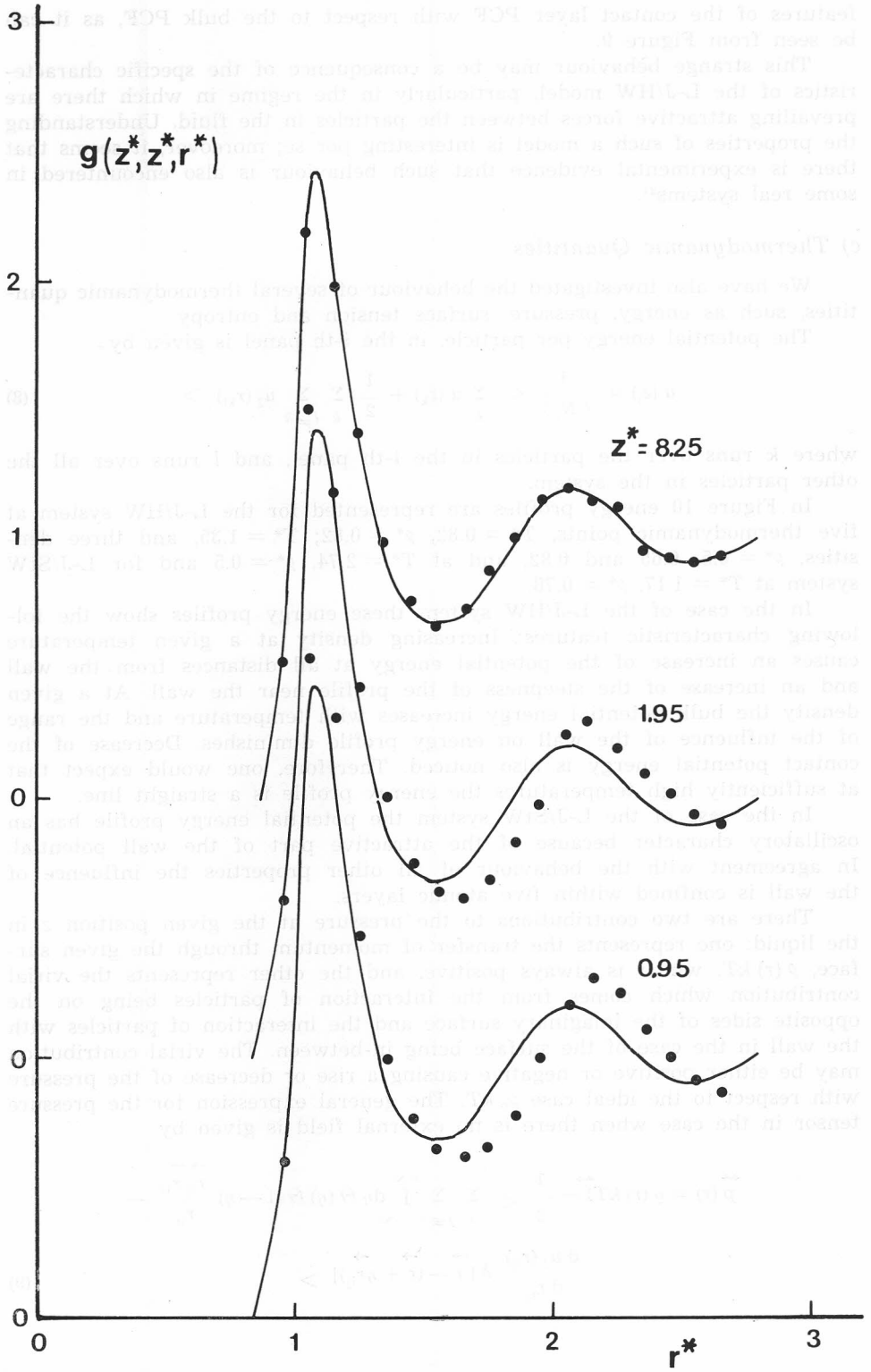

Figure 9. PCF's for L-J/StW at $T^* = 1.17$ and $\varrho^* = 0.78$ for various distances z^* from the wall (dots) and the bulk PCF (full line).

features of the contact layer PCF with respect to the bulk PCF, as it can be seen from Figure 9.

This strange behaviour may be a consequence of the specific characteristics of the L-J/HW model, particularly in the regime in which there are prevailing attractive forces between the particles in the fluid. Understanding the properties of such a model is interesting per se; moreover, it seems that there is experimental evidence that such behaviour is also encountered in some real systems[21].

c) *Thermodynamic Quantities*

We have also investigated the behaviour of several thermodynamic quantities, such as energy, pressure, surface tension and entropy.

The potential energy per particle, in the i-th panel is given by

$$u(z_i) = \frac{1}{\langle N_i \rangle} < \sum_k u(z_k) + \frac{1}{2} \sum_k \sum_{l \neq k} u_2(r_{kl}) > \tag{8}$$

where k runs over the particles in the i-th panel, and l runs over all the other particles in the system.

In Figure 10 energy profiles are represented for the L-J/HW system at five thermodynamic points, $T^* = 0.82$, $\rho^* = 0.82$; $T^* = 1.35$, and three densities, $\rho^* = 0.5$, 0.65 and 0.82, and at $T^* = 2.74$, $\rho^* = 0.5$ and for L-J/StW system at $T^* = 1.17$, $\rho^* = 0.78$.

In the case of the L-J/HW system these energy profiles show the following characteristic features: Increasing density at a given temperature causes an increase of the potential energy at all distances from the wall and an increase of the steepness of the profile near the wall. At a given density the bulk potential energy increases with temperature and the range of the influence of the wall on energy profile diminishes. Decrease of the contact potential energy is also noticed. Therefore, one would expect that at sufficiently high temperatures the energy profile is a straight line.

In the case of the L-J/StW system the potential energy profile has an oscillatory character because of the attractive part of the wall potential. In agreement with the behaviour of all other properties the influence of the wall is confined within five atomic layers.

There are two contributions to the pressure at the given position z in the liquid; one represents the transfer of momentum through the given surface, $\rho(r)\, kT$, which is always positive, and the other represents the virial contribution which comes from the interaction of particles being on the opposite sides of the imaginary surface and the interaction of particles with the wall in the case of the surface being in-between. The virial contribution may be either positive or negative causing a rise or decrease of the pressure with respect to the ideal case $\rho_b\, kT$. The general expression for the pressure tensor in the case when there is no external field is given by

$$\overleftrightarrow{p}(r) = \varrho(r)\, kT \overleftrightarrow{1} - \frac{1}{2} < \sum_i \sum_{j \neq i} \int_{-\infty}^{+\infty} d\eta\, \Theta(\eta)\, \Theta(1-\eta)\, \frac{\vec{r}_{ij}\, \vec{r}_{ij}}{|r_{ij}|} - \frac{d\, u_2(r_{ij})}{d\, r_{ij}}\, \delta[\vec{r} - (\vec{r} + \eta \vec{r}_{ij})] > \tag{9}$$

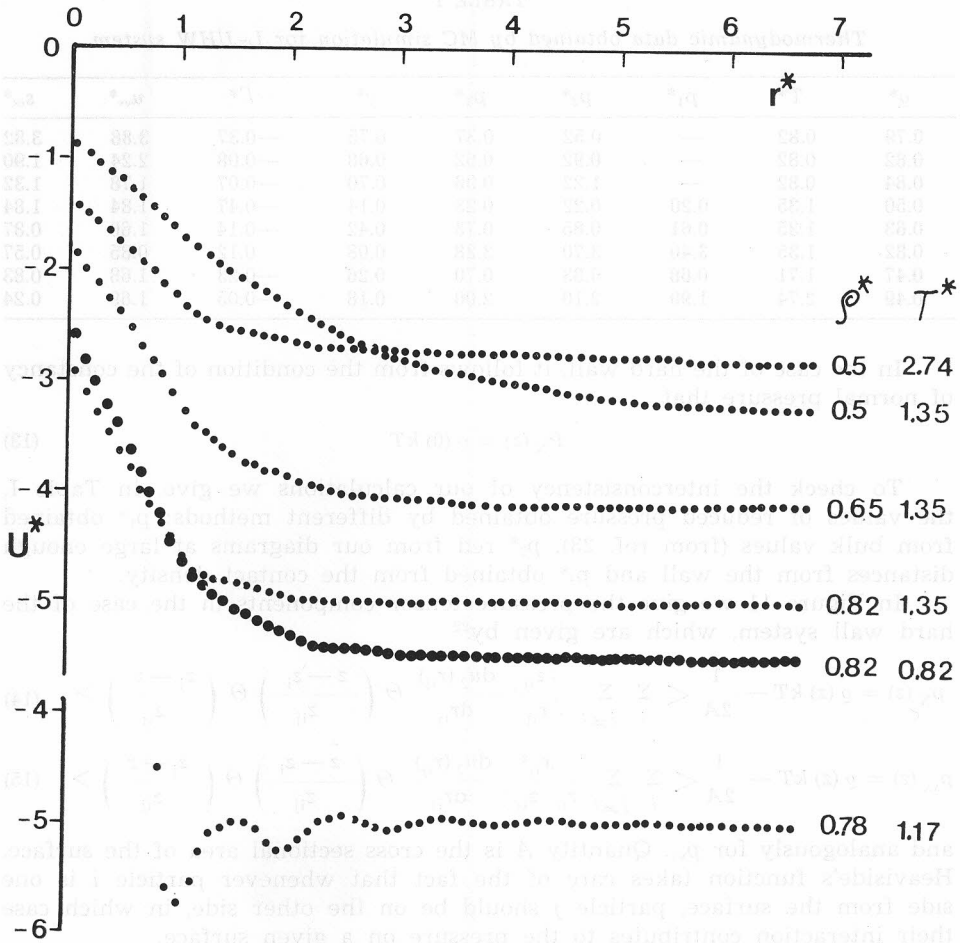

Figure 10. Profiles of the potential energy per particle for L-J/HW at various points and the bottom curve for L-J/StW.

where $\Theta(\eta)$ is the Heaviside step function. For details concerning eq. (9) see ref. 22.

From the condition of mechanical equilibrium we can deduce that the normal component of the pressure tensor does not vary with the distance from the wall, *i. e.*

$$p_N(z) = p_{zz}(z) = \text{const.} \tag{10}$$

while the tangential components satisfy the following equation

$$\frac{\partial p_{xx}}{\partial x} = \frac{\partial p_{yy}}{\partial y} = 0 \tag{11}$$

giving

$$p_T(z) = \frac{1}{2}(p_{xx}(z) + p_{yy}(z)) \tag{12}$$

to be an unknown function of z only.

TABLE I

Thermodynamic data obtained by MC simulation for L-J/HW system

ϱ^*	T^*	p_1^*	p_2^*	p_3^*	γ^*	Γ^*	u_{ex}^*	s_{ex}^*
0.79	0.82	—	0.52	0.37	0.75	—0.37	3.88	3.82
0.82	0.82	—	0.92	0.62	0.68	—0.08	2.24	1.90
0.84	0.82	—	1.22	0.96	0.70	—0.07	1.78	1.32
0.50	1.35	0.20	0.22	0.23	0.14	—0.47	1.84	1.84
0.63	1.35	0.61	0.85	0.73	0.42	—0.14	1.60	0.87
0.82	1.35	3.40	3.70	3.38	0.08	0.12	0.85	0.57
0.47	1.71	0.68	0.83	0.70	0.26	—0.23	1.68	0.83
0.49	2.74	1.99	2.10	2.00	0.18	—0.05	1.69	0.24

In the case of the hard wall, it follows from the condition of the constancy of normal pressure that

$$P_N(z) = \varrho(0)\, kT \tag{13}$$

To check the interconsistency of our calculations we give, in Table I, the values of reduced pressure obtained by different methods: p_1^* obtained from bulk values (from ref. 23), p_2^* red from our diagrams at large enough distances from the wall and p_3^* obtained from the contact density.

In Figure 11 we give the pressure tensor components in the case of the hard wall system, which are given by[22]

$$p_N(z) = \varrho(z)\, kT - \frac{1}{2A} \left\langle \sum_i \sum_{j \neq i} \frac{|z_{ij}|}{r_{ij}} \frac{du_2(r_{ij})}{dr_{ij}} \Theta\left(\frac{z - z_i}{z_{ij}}\right) \Theta\left(\frac{z_j - z}{z_{ij}}\right) \right\rangle \tag{14}$$

$$p_{xx}(z) = \varrho(z)\, kT - \frac{1}{2A} \left\langle \sum_i \sum_{j \neq i} \frac{x_{ij}^2}{r_{ij} |z_{ij}|} \frac{du_2(r_{ij})}{dr_{ij}} \Theta\left(\frac{z - z_i}{z_{ij}}\right) \Theta\left(\frac{z_j - z}{z_{ij}}\right) \right\rangle \tag{15}$$

and analogously for p_{yy}. Quantity A is the cross sectional area of the surface. Heaviside's function takes care of the fact that whenever particle i is one side from the surface, particle j should be on the other side, in which case their interaction contributes to the pressure on a given surface.

From Figure 11 it can be seen that $p_N(z)$ is quite constant with z, as expected from eq. (10). On the other hand, p_{xx} and p_{yy} have large oscillations with z. The integral over the difference of the normal and tangential component of the pressure gives the surface tension

$$\gamma = \int [p_T(z) - p_N(z)]\, dz \tag{16}$$

where integration ranges over the interface region. This value is also given in Table I. Unfortunately, the uncertainty of the data is to high so that we are not in a position to give a decisive conclusion, although it seems that the surface tension has maximum values around the transition straight line shown in Figure 1. We should emphasize once more that we are talking about the solid-liquid surface tension and not the liquid-gas one, which is usually on one's mind when speaking about surface tension. About the solid--liquid surface tension not much is known from either theoretical or experimental points of view.[24] Our calculation is that of a very specific model of the structureless wall. In the case of the hard sphere/hard wall (HS/HW)

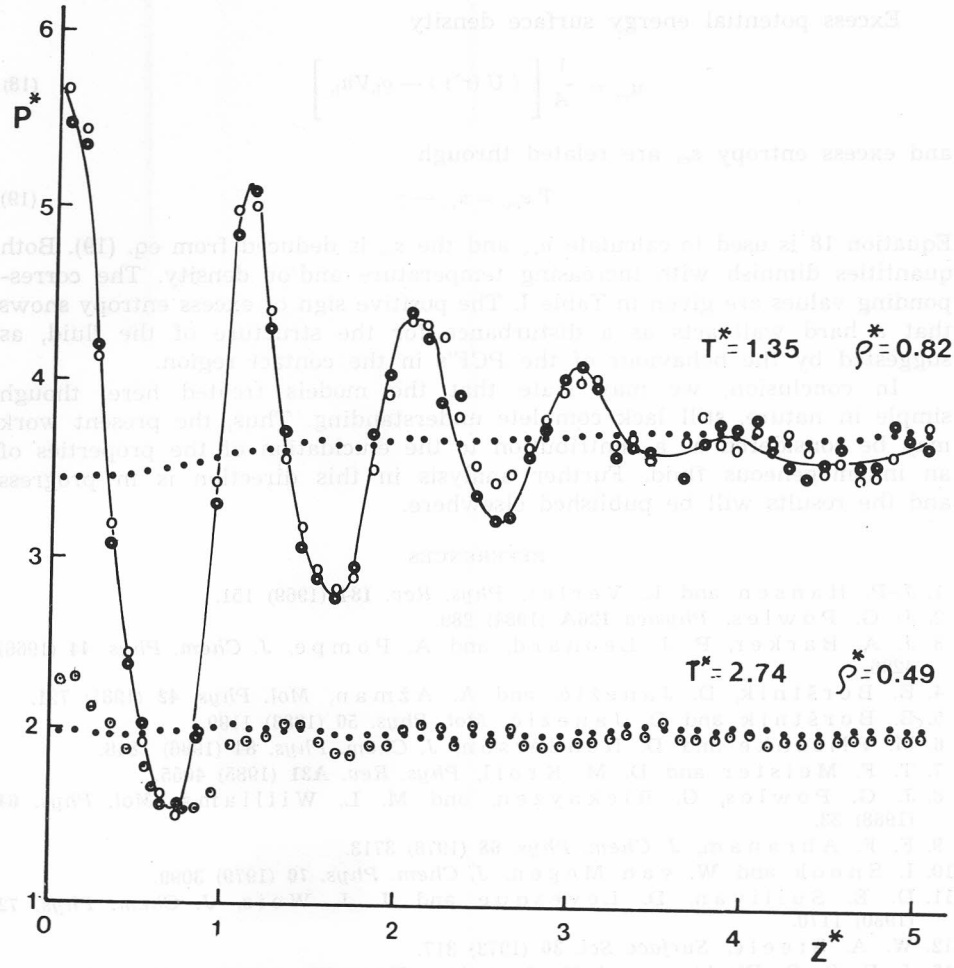

Figure 11. Profiles of pressure tensor components for L-J/HW. Dots represent the $p_N = p_{zz}$ component, while ● is p_{xx}, ○ p_{yy} and ⊙ p_T. The full curve is the guide eye passing through p_{xx} and p_{yy}.

system the calculation[18] gives negative values for γ. In the case of the structured wall Ladd and Woodcock[25] give a value which is significantly smaller. Toxvaerd[26] found that for a L-J fluid in contact with a plane of L— particles or with a mean field plane, interacting through 10—4 L-J potential with fluid particles, there is an increase of surface tension with increasing density.

Excess number density $\Gamma = N_{ex}/A$ defined by

$$\Gamma = \Delta z \left[\sum_i \varrho(z_i) - i\,\varrho_b \right] \tag{17}$$

and the reduced value $\Gamma^* = \Gamma\sigma^2$ for several thermodynamic points are given in Table I. For our system Γ^* is mainly negative and becomes positive for highly pronounced oscillatory profiles.

Excess potential energy surface density

$$u_{ex} = \frac{1}{A}\left[\langle U(r^N) \rangle - \varrho_b V u_b \right] \tag{18}$$

and excess entropy s_{ex} are related through

$$T e_{ex} = u_{ex} - \gamma \tag{19}$$

Equation 18 is used to calculate u_{ex} and the s_{ex} is deduced from eq. (19). Both quantities dimnish with increasing temperature and/or density. The corresponding values are given in Table I. The positive sign of excess entropy shows that a hard wall acts as a disturbance for the structure of the fluid, as suggested by the behaviour of the PCF's in the contact region.

In conclusion, we may state that the models treated here, though simple in nature, still lack complete understanding. Thus, the present work may be considered as a contribution to the elucidation of the properties of an inhomogeneous fluid. Further analysis in this direction is in progress and the results will be published elsewhere.

REFERENCES

1. J.-P. Hansen and L. Verlet, *Phys. Rev.* **184** (1969) 151.
2. J. G. Powles, *Physica* **126A** (1984) 289.
3. J. A. Barker, P. J. Leonard, and A. Pompe, *J. Chem. Phys.* **44** (1966) 4206.
4. B. Borštnik, D. Janežić, and A. Ažman, *Mol. Phys.* **42** (1981) 721.
5. B. Borštnik and D. Janežič, *Mol. Phys.* **50** (1983) 1199.
6. M. Plischke and D. Henderson, *J. Chem. Phys.* **84** (1986) 2846.
7. T. F. Meister and D. M. Kroll, *Phys. Rev.* **A31** (1985) 4055.
8. J. G. Powles, G. Rickayzen, and M. L. Williams, *Mol. Phys.* **64** (1988) 33.
9. F. F. Abraham, *J. Chem. Phys.* **68** (1978) 3713.
10. I. Snook and W. van Megen, *J. Chem. Phys.* **70** (1979) 3099.
11. D. E. Sullivan, D. Levesque and J. J. Weis, *J. Chem. Phys.* **72** (1980) 1170.
12. W. A. Steele, *Surface Sci.* **36** (1973) 317.
13. J. P. R. B. Walton and N. Quirke, *Chem. Phys. Letters* **129** (1986) 382.
14. G. Balabanić, F. Sokolić, R. Milčić, and A. Rubčić, *Farm. Vestnik* **38** (1987) 187.
15. L. Verlet, *Phys. Rev.* **165** (1968) 201.
16. G. Balabanić, B. Borštnik, R. Milčić, A. Rubčić, and F. Sokolić, *Springer Proceedings in Physics,* Vol. 40, (Editors: M. Davidović and A. K. Soper), Springer-Verlag, 1989. *Proceedings of the International Workshop on Static and Dynamic Properties of Liquids,* Dubrovnik, June 27 — July 1, 1988.
17. I. K. Snook and D. Henderson, *J. Chem. Phys.* **68** (1978) 2134.
18. J. R. Henderson and F. van Swol, *Mol. Phys.* **51** (1984) 991.
19. J. R. Grigera, *J. Chem. Phys.* **72** (1980) 3439.
20. R. D. Groot, *Mol. Phys.* **60** (1987) 45.
21. A. K. Sopper, private communication (1988).
22. M. Rao and B. J. Berne, *Mol. Phys.* **37** (1979) 455.
23. J. A. Barker and D. Henderson, *Rev. Mod. Phys.* **48** (1976) 587.
24. D. P. Woodruff, *The Solid-Liquid Interface,* Cambridge Univ. Press, 1973.
25. A. J. C. Ladd and L. V. Woodcock, *Mol. Phys.* **36** (1978) 611.
26. S. Toxvaerd, *J. Chem. Phys.* **74** (1981) 1998.

SAŽETAK

Istraživanje graničnog područja čvrsto-tekuće pomoću kompjutorske simulacije

G. Balabanić, B. Borštnik, R. Milčić, A. Rubčić i F. Sokolić

Metoda Monte Carlo primijenjena je u istraživanju dvaju modela za granično područje čvrsto-tekuće: Lennard-Jones-ov fluid u dodiru s čvrstom i mekom stijenkom. Da se objasni ponašanje fluida u graničnom području izračunane su slijedeće fizičke veličine: profili gustoće, parne korelacijske funkcije, profili potencijalne energije i komponenata tenzora tlaka, površinska napetost te vrijednosti odstupanja od homogenog fluida za gustoću čestica, potencijalnu energiju i entropiju po jedinici površine. Sve su te veličine izračunane u različitim termodinamičkim točkama faznog dijagrama, da bi se odredila njihova zavisnost o temperaturi i gustoći sistema. Neočekivan rezultat je da uređenost Lennard-Jones-ova fluida opada pokraj čvrste stijenke, a raste uz meku stijenku.